IEEE Access
Multidisciplinary | Rapid Review | Open Access Journal

Received December 16, 2020, accepted December 28, 2020, date of publication January 1, 2021, date of current version January 12, 2021.

Digital Object Identifier 10.1109/ACCESS.2020.3048723

Consensus-Based Delay-Tolerant Distributed Secondary Control Strategy for Droop Controlled AC Microgrids

SHAFAAT ULLAH[1,2], LAIQ KHAN[3], IRFAN SAMI[4], AND NASIM ULLAH[5]

[1]Department of Electrical Engineering, University of Engineering and Technology Peshawar, Bannu Campus, Bannu 28100, Pakistan
[2]Department of Electrical and Computer Engineering, COMSATS University Islamabad, Abbottabad Campus, Abbottabad 22060, Pakistan
[3]Department Electrical and Computer Engineering, COMSATS University Islamabad, Islamabad 45550, Pakistan
[4]School of Electrical and Electronics Engineering, Chung-Ang University, Seoul 06974, South Korea
[5]Department of Electrical Engineering, College of Engineering, Taif University, Taif 21944, Saudi Arabia

Corresponding author: Nasim Ullah (nasimullah@tu.edu.sa)

This research work was supported by Taif University Researchers Supporting Project number (TURSP-2020/144), Taif University, Taif, Saudi Arabia.

ABSTRACT This article formulates a fully-distributed and delay-tolerant secondary control scheme for droop-controlled AC microgrids. The proposed strategy is inspired by the cooperative control concept of multi-agent systems (MASs). It considers the hierarchical control structure of the distributed energy resource (DER) units. It ensures equal active power sharing between three DER units, where each unit tracks the time-varying average load, with a finite-time convergence. As a result, the frequencies of the DER units are regulated to their nominal values. Furthermore, it offers plug-and-play capability for DER units, demonstrates significant robustness against load disturbances, and successfully tolerates, small as well as large, communication time-delays. Due to the fully-distributed configuration of the proposed control strategy, each DER unit in the test microgrid requires only its own information and information of its neighbors. The benefit is two-fold: not only this configuration assists in minimizing the overall bandwidth requirement, and cost of the corresponding communication network, but also it increases the reliability of the microgrid operation. The performance and effectiveness of the proposed technique is supported by exhaustive numerical simulations performed in Matlab/Simulink on an AC microgrid testbench comprising three DER units. The proposed strategy renders the superior performance in several aspects as compared to the existing developments in the literature in this area.

INDEX TERMS Plug-and-play, droop control, microgrid, consensus, cooperative control, graph theory, Laplacian, distributed control, finite-time, multi-agent system.

I. INTRODUCTION

GENERALLY, a low voltage, small-scale electric power grid is termed as a microgrid. It comprises distributed generation (DG) units (such as photovoltaic systems, solar-thermal systems, wind turbines, fuel cells, geothermal systems, low-head hydro units, internal combustion engines and mini- and micro-gas-turbines), distributed energy storage (DES, such as battery energy storage, super capacitor or ultra capacitor storage, superconducting magnetic energy storage systems and low- and high-speed flywheel systems) and loads interconnected through power lines. A DG unit may either be interfaced through a power electronic converter or directly through an AC rotating machine. The DG units with the power electronic interface provide low inertia, high speed/fast response time and flexibility for controlling the output voltage, frequency, and active/reactive power of the unit. The DG and DES units are collectively known as the distributed energy resources (DERs). A microgrid must be capable of solving energy issues locally. It can be operated either in islanded (i.e., autonomous) or grid-connected mode [1]–[4].

The microgrid possesses a hierarchical control scheme that comprises primary/inner control (droop control), secondary control and tertiary control levels [5]. Under normal operation, the microgrid remains connected to the main grid. However, it will switch to the autonomous mode in case of

The associate editor coordinating the review of this manuscript and approving it for publication was Elizete Maria Lourenco.

some disturbance. Hence, a suitable control scheme, capable of keeping the frequency/voltage stabilized and maintaining active/reactive power sharing, is crucial for stable and economically efficient operation of the microgrid. Both the frequency and voltage of the microgrid are dictated by the main grid in the grid-connected mode, however, in the islanded mode, the primary control takes the responsibility of the frequency and voltage control [6]–[9]. The operation of the microgrid with the primary control layer alone, in the islanded mode, causes the steady-state load-dependent frequency and voltage deviations, giving rise to power quality issues and deteriorating the healthy operation of the microgrid. Thus, it needs to compensate for these deviations by the deployment of an additional secondary control layer in order to restore the frequency and voltage of each DER unit back to its nominal (i.e., reference or standard) value [10]–[13].

The secondary control strategies include centralized control (having low reliability due to single point of failure) [14], [15], decentralized control (having high reliability together with reasonable cost) [15]–[17] and distributed control (having high reliability along with low cost) [15], [18], [19]. The distributed control concept is inspired by the cooperative control concept of multi-agent systems (MASs). It is based on communication among local controllers capable of exchanging information with the neighboring agents through local communication networks [20], [21]. The DER unit in a microgrid is regarded as an agent capable of communicating with its neighboring agents (other DER units) through a sparse communication network. Thus, the microgrid behaves as a MAS. The conventional secondary control scheme of AC microgrids exploits a centralized structure, in which each node (i.e., DER unit) remains bidirectionally connected to all the remaining nodes. This controller issues global commands to gather system-wide information, thus requiring a complex and costly communication network, lacking flexibility and prone to single point of failure. That is, the centralized control strategy stops working no matter whether a single node breaks down from or loses connection to the remaining communication network, caused by the communication link failure [13], [22], [23]. Conversely, the main advantage of the distributed control strategy is that a node is not necessarily needed to communicate with all the other nodes in the communication network, thus reducing the cost and bandwidth requirement of the communication network and enhancing the reliability of the overall microgrid operation. Due to this attribute, the distributed cooperative control strategies are quite popular for providing promising solutions in microgrid and smart grid applications [24].

A wide variety of distributed cooperative secondary control strategies can be found in the existing scientific literature. Such as, in [13], a consensus-based robust secondary frequency and voltage restoration along with active power sharing control strategy has been implemented for an islanded AC microgrid based on a prototype IEEE 14-bus system. The proposed strategy has been found superior to distributed cooperative secondary voltage control of microgrids using feedback linearization, reported in [25] by effectively handling frequent switching communication topologies, parametric uncertainties, plug-and-play feature, load disturbances and communication time-delays. Since, the dynamics of DGs in a microgrid are nonlinear and heterogeneous (i.e., non-identical), hence, input–output feedback linearization strategy was implemented to convert the nonlinear heterogeneous dynamics of DGs to linear dynamics in [25]. However, it ignored the dynamics of the primary controller that might decline both the performance and stability of the microgrid operation. Then, in [26], the same group of researchers, in the sequel, developed a multi-agent consensus-based distributed cooperative control strategy for secondary frequency and voltage control of inverter-interfaced microgrids. Since, in both [25], [26], the minimum real part of the non-zero eigenvalue of the graph Laplacian matrix was directly involved in the proposed control law, which was a global information, thus, indicating that the proposed control schemes were not fully-distributed. This issue has been addressed in [27] by developing a distributed adaptive (commonly known as fully-distributed) cooperative control framework for droop-controlled islanded AC microgrid. The authors in [24] have proposed a finite-time robust distributed secondary voltage and frequency control technique for inverter-interfaced DGs in an islanded AC microgrid that demonstrated accurate active power sharing between four DGs. The proposed technique has been found to offer plug-and-play feature, and robustness to reconfiguration of the communication network structure, parametric uncertainties and unmodeled system dynamics. In [15], the authors have developed a droop-based distributed cooperative control technique for an islanded AC microgrid, comprising five DGs. The frequencies, voltage magnitudes, and active/reactive powers of all the DGs were regulated to the desired reference values under both fixed and switching communication network topology with non-uniform time-varying delays. The closed-loop system response becomes oscillatory, or even unstable, when the communication time-delay exceeds a certain extent, as reported in [13], [28]. The idea of distributed-averaging proportional-integral (DAPI) controller has been introduced, in [29], and implemented for secondary frequency and voltage control of islanded AC microgrid, comprising four inverter-interfaced DG units. An extensive literature review on the decentralized, distributed and hierarchical control schemes has been reported in [12], covering droop-controlled islanded as well as grid-connected microgrids. A significant investigation has been carried out in [28] to demonstrate the effect of communication time-delays on the secondary frequency control of an islanded AC microgrid based on Canadian urban distribution system with multiple DG units. It has been reported that the communication delay margin increases with the increase in the proportional gains of the secondary frequency controller. However, it decreases with the increase in the integral gains. The communication delay effect was counteracted by a gain scheduling approach.

A. MOTIVATION AND SIGNIFICANT CONTRIBUTIONS

The existing developments and limitations found in the literature motivated the authors to propose a fully-distributed multi-agent consensus-based secondary control scheme for achieving multiple objectives, simultaneously. The major contributions of the article are summarized below:

1) A fully-distributed and robust secondary frequency and equal active power sharing control framework is proposed for an AC microgrid that ensures equal active power sharing between DER units, and in turn regulates their frequencies to the nominal value in a finite-time.
2) The proposed control scheme ensures equal active power sharing and frequency regulation using a single control protocol for each DER unit as compared to the concepts reported in [13], [30]–[32], where a separate control methodology has been used for both purposes.
3) The proposed strategy, being fully-distributed, requires only the local information, that is, information of each constituent DER unit and its neighbors, but not about the entire network. This feature of the proposed technique in turn minimizes the overall bandwidth requirement. Furthermore, it offers greater reliability and flexibility for microgrid operation.
4) The proposed strategy successfully tolerates both small as well as large communication time-delays and ensures proper operation.
5) The proposed scheme offers plug-and-play feature for the DER units.

This article is categorized as follows: the introduction and background literature review is covered in Section I. Section II presents preliminaries on algebraic graph theory. Section III covers the mathematical modeling of each constituent DER unit of the test microgrid. Section IV describes the proposed fully-distributed and delay-tolerant secondary control strategy design. Section V presents performance validation of the proposed technique through exhaustive numerical simulations carried out in Matlab/Simulink, and, finally, Section VI concludes this article with the concluding remarks.

II. PRELIMINARY ALGEBRAIC GRAPH THEORY

A microgrid itself is conceptualized as a MAS, where the DER units play the role of communicating agents or nodes or vertices, while the communication links are viewed as edges. Each DER unit can communicate/share information with its neighboring DER units through a sparse communication network. The communication among different agents (DER units in this case) in a MAS, consisting of N agents, is indicated graphically by a directed (one-way) or undirected (two-way) communication graph, $\mathcal{G}$, and its explanation is covered using algebraic graph theory [13]. Mathematically, this graph, $\mathcal{G}$, can be described by a weighted Laplacian matrix, $L \triangleq \left[\ell_{ij}\right] \in \mathbb{R}^{N\times N}$, where the diagonal and off-diagonal entries are expressed as follows [30]:

$$L \triangleq \left[\ell_{ij}\right] \quad \text{where} \quad \ell_{ij} \triangleq \begin{cases} d_i^{in} = \sum\limits_{j\in\mathcal{N}_i} a_{ij} & \forall \quad i = j \\ -a_{ij} & \forall \quad i \neq j \end{cases} \tag{1}$$

where d_i^{in} is the in-degree of agent i (i.e., the number of neighboring agents it is connected to/receiving information from or the number of edges terminating at node i), $j \in \mathcal{N}_i$ represents the set of neighboring agents of agent i, and a_{ij} is the weight of the communication link (or the number of edges) between agent i and j. Note that the element $a_{ij} > 0$ if node i is receiving information from node j (i.e., information flow is from node j to node i), otherwise $a_{ij} = 0$. Another strategy for obtaining the Laplacian matrix of the communication graph, $\mathcal{G}$, is by using: $L \triangleq D^{in} - A$, where $D^{in} \triangleq diag\left\{d_i^{in}\right\} \in \mathbb{R}^{N\times N}$ and $A \triangleq \left[a_{ij}\right] \in \mathbb{R}^{N\times N}$ are, respectively, the diagonal weighted in-degree matrix and non-negative weighted adjacency matrix, with their entries defined as follows:

$$A \triangleq \left[a_{ij}\right] \quad \text{where} \quad a_{ij} \triangleq \begin{cases} 0 & \forall \quad i = j \\ > 0 & \forall \quad i \neq j \end{cases} \tag{2}$$

$$D^{in} \triangleq diag\left\{d_i^{in}\right\} \quad \text{where} \quad d_i^{in} \triangleq \sum_{j\in\mathcal{N}_i} a_{ij} \quad \forall \quad i = j \tag{3}$$

The in-degree matrix, D^{in}, is a diagonal matrix with its diagonal entries representing the in-degree, d_i^{in}, of agent i, while rest of the off-diagonal entries are 0. Conversely, all the diagonal entries of the adjacency matrix, A, are equal to 0, while rest of the off-diagonal entries are non-negative. The out-degree of a node i, indicated by d_i^{out}, where $d_i^{out} = \sum_{i\in\mathcal{N}_j} a_{ji}$ and $D^{out} \triangleq diag\left\{d_i^{out}\right\} \in \mathbb{R}^{N\times N}$, represents the number of neighboring agents it is sending information to. When $d_i^{in} = d_i^{out}$, for all nodes in the communication network, the communication graph, $\mathcal{G}$, is termed as balanced. When $a_{ij} = a_{ji}$, that is if there is a two-way/bidirectional communication link between nodes i and j having the same weights in both directions, the communication graph, $\mathcal{G}$, is known as undirected.

III. MATHEMATICAL MODELING OF DER UNITS INCLUDING PRIMARY/DROOP CONTROL

After theoretical development, the feasibility and effectiveness of the proposed secondary control strategy has been tested on a three-phase AC microgrid testbed, as shown in Fig. 1. The communication between DER units is represented by blue double-headed dotted arrows. This microgrid has four buses, two inverter-based DER units (i.e., an external energy storage system (ESS) and a microsource (MS)), and an internal combustion (IC) engine driven wound-field synchronous generator-based diesel genset (GS). The ESS, MS and GS are connected to bus 1, 3 and 4, respectively, via ΔY-transformers. The microgrid itself is connected to the main grid at bus 1 through a static switch (SS). The sources are connected through transformers, series coupling

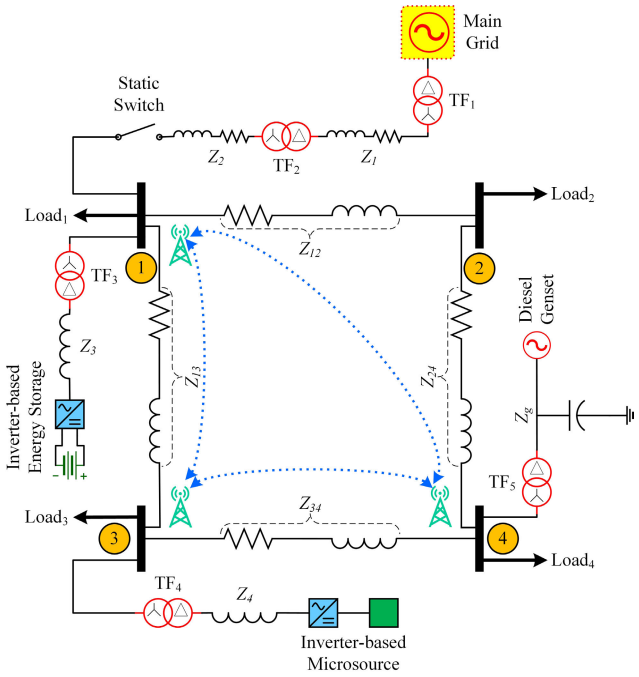

FIGURE 1. AC microgrid testbed.

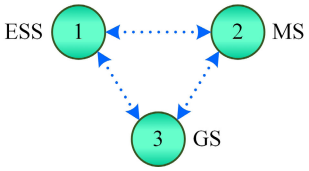

FIGURE 2. Communication graph.

inductances (Z_3 and Z_4) and coupling capacitor (Z_g) to the buses, while loads are connected directly to the buses. The lines (Z_1, Z_2, Z_{12}, Z_{13}, Z_{24} and Z_{34}) are modeled as series RL branches. The overall parameters of the testbed and the main grid are specified in Tables 1, 2, 3 and 4 in Appendix. The DER units communicate with each other through the undirected communication graph, $\mathcal{G}$, depicted in Fig. 2.

A. MATHEMATICAL MODELING OF INVERTER-BASED MICROSOURCE WITH PRIMARY/DROOP CONTROL AND OVERLOAD MITIGATION STRATEGY

The inverter-interfaced MS can be modeled as a three-phase controlled voltage source, whose frequency and voltage magnitude can be set through external inputs, that is, the desired frequency and magnitude of the desired peak line-to-neutral (or phase) voltage at the inverter terminals (i.e., ω and V_{pk}, respectively). The outputs are instantaneous three-phase voltages (v_a, v_b and v_c), as described below [33]:

$$\begin{aligned} v_a &= V_{pk}\sin(\omega t + 0^\circ) \\ v_b &= V_{pk}\sin\left(\omega t - 120^\circ\right) \\ v_c &= V_{pk}\sin\left(\omega t + 120^\circ\right) \end{aligned} \tag{4}$$

where $V_{pk} = M_d V_{DC}$, with M_d representing the modulation index, and V_{DC} the inverter's DC input voltage.

1) PRIMARY/DROOP CONTROL

The inverter-interfaced MS, as a controlled voltage source, is depicted in Fig. 3, including its primary/droop control. The $P\omega$-droop control for MS can be expressed as follows:

$$\omega = \omega_{base} + \Delta\omega_{adj} + m_P\left(P_{req} - P_{meas}\right) \tag{5}$$

where ω is the frequency of the inverter-based MS, $\omega_{base} = \omega_0$ is the nominal microgrid frequency, $\Delta\omega_{adj}$ is the frequency adjustment under overload mitigation strategy, m_P is the droop gain (slope of the $P\omega$-droop curve), $P_{req} = P_{set}$ is the MS active power set-point, and P_{meas} is the instantaneous measured active power.

For a frequency droop of, $\Delta\omega = \pi$ rad or $\Delta f = 0.5$ Hz, the $P\omega$-droop characteristic slope, m_P, is calculated as follows:

$$\left.\begin{aligned} m_P &= \frac{\Delta\omega}{\Delta P} = \frac{2\pi\Delta f}{P_{max} - P_{min}} \\ &= \frac{2\pi\ (0.5)}{1\ (\text{pu}) - 0\ (\text{pu})} = \pi\ \text{rad/pu} \end{aligned}\right\} \tag{6}$$

This value of m_P allows the MS for an active power request within its power range and this operation occurs within the limit of ± 0.5 Hz of the normal operating frequency range.

During parallel operation with the main grid, the active power of the MS is regulated to a desired value. However, during an islanding event, the $P\omega$-droop controller ensures autonomous active load tracking, by adjusting the frequency of the MS, ω. Such that, during an islanding event, there is a loss of active power from the main grid. So, this loss of power must be supplied by the DER units locally in the microgrid. The $P\omega$-droop controller calculates the instantaneous active power and reduces the inverter's output frequency as prescribed by the $P\omega$-droop characteristic [34], [35]. As a result, the MS will immediately ramp up its active power output to match the missing quota of active power from the main grid, without using any explicit communication with the other sources.

Similarly, the QV-droop control for MS can be expressed as follows:

$$V_{pk} = V_{req} - V_{meas} - m_Q Q_{meas} \tag{7}$$

where $V_{req} = V_{set}$ is the MS line-to-neutral voltage magnitude set-point, V_{meas} is instantaneous measured line-to-neutral voltage, m_Q is the droop gain (slope of the QV-droop curve), and Q_{meas} is the instantaneous measured reactive power.

The voltage magnitude is allowed to droop by 5 % for every 1 pu change in reactive power, for which the QV-droop characteristic slope, m_Q, is calculated as follows:

$$\left.\begin{aligned} m_Q &= \frac{\Delta V}{\Delta Q} = \frac{\Delta V}{Q_{max} - Q_{min}} = \frac{0.05}{1\ (\text{pu}) - 0\ (\text{pu})} \\ &= 0.05\ \text{V/pu} \end{aligned}\right\} \tag{8}$$

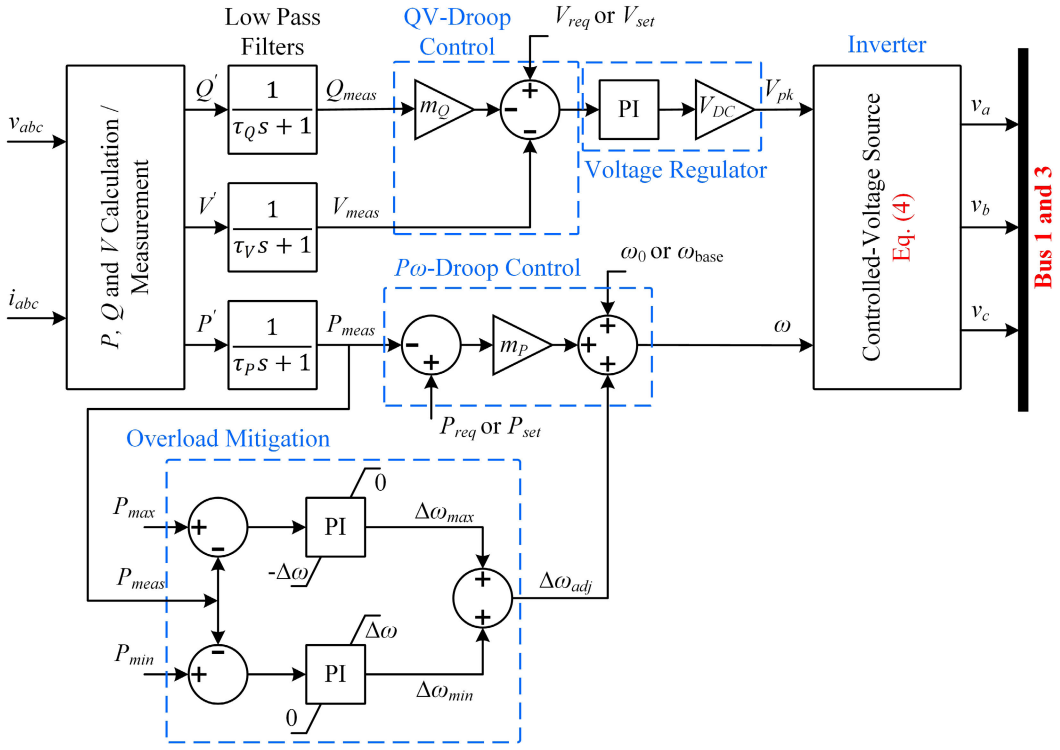

FIGURE 3. Inverter-interfaced microsource with its primary/droop control and overload mitigation strategy.

For example, injecting 0.1 pu of capacitive reactive power, the voltage will be allowed to sag 0.5 %. Although, it seems a very small correction, but it results in a great deal of limiting the amount of reactive power injection.

The main function of the QV-droop controller is to adjust the externally requested voltage magnitude to that value that will require less injection of the reactive power from the MS [35].

2) OVERLOAD MITIGATION STRATEGY

In a microgrid, when one of the grid-forming AC sources reaches its power limits, while the others have not, then a sudden load change event may overload that particular grid-forming source that have already reached its power limits. A prolonged overload may stall the IC engine or damage the ESS, which may eventually collapse the overall microgrid. This overloading condition can be mitigated by shifting the extra load from the overloaded source, by reducing/adjusting its own frequency, to those sources which have not yet reached their power limits [35]. Because, active power always flows from a source with higher frequency towards the one having a lower frequency. This overload mitigation strategy, indicated in Fig. 3, operates autonomously without requiring any communication. Its main advantage is to maintain voltage control of the grid-forming source during load transient by redistributing the power flow in the microgrid, and it does not require switching between the grid-forming and grid-following control.

During overload mitigation, the active power limits of the MS (i.e., P_{min} and P_{max}) must be enforced. These limits are controlled through the maximum and minimum frequency limits of two PI controllers. The outputs of both the PI-controllers (i.e., $\Delta\omega_{max}$ and $\Delta\omega_{min}$) are zero, when the MS operates within its power limits. There is a zero upper limit of the upper PI controller, indicating that the controller will only be activated when the active power output of the MS exceeds P_{max}. So, when P_{max} is exceeded, then $\Delta\omega_{max}$ becomes negative (i.e., never positive) to enforce the power limit. There is also a lower $-\Delta\omega$ limit of the upper PI controller, for avoiding the active power output of the MS being less than P_{min}, which in turn protects the MS frequency from dropping too much during sudden load transient. Thus, when the droop-controlled MS becomes overloaded, the upper PI controller will be activated and it will reduce the frequency of the MS rapidly to mitigate its overload. Conversely, for avoiding the active power output of the MS being less than P_{min}, a downward PI controller with a $\Delta\omega$ upper limit and a zero lower limit is also introduced. So, when $P_{min} = 0$ is exceeded, then $\Delta\omega_{min}$ becomes positive (i.e., never negative) to enforce the power limit. In this way, the output of each PI controller, in the overload mitigation block, will regulate the frequency of the overloaded MS [34]–[36].

B. MATHEMATICAL MODELING OF INVERTER-BASED EXTERNAL ENERGY STORAGE SYSTEM WITH PRIMARY/DROOP CONTROL AND OVERLOAD MITIGATION STRATEGY

The inverter-interfaced ESS also can be modeled as a 3-phase controlled voltage source, and its mathematical

model with primary/droop control and overload mitigation strategy is the same as that of the inverter-interfaced MS, with one significant difference. For ESS, the minimum active power, P_{min}, is set to a negative value, that is, $P_{min} = -2.5\,\text{kW} = -0.1667$ pu, to give an indication of the energy storage/battery charging. This makes the slope, m_P, of the $P\omega$-droop characteristic for the ESS, different from that of the MS, as follows:

$$\left.\begin{aligned} m_P &= \frac{\Delta\omega}{\Delta P} = \frac{2\,\pi\,\Delta f}{P_{max} - P_{min}} \\ &= \frac{2\,\pi\,(0.5)}{1\,(\text{pu}) - (-0.1667)\,(\text{pu})} = 2.6928\,\text{rad/pu} \end{aligned}\right\} \quad (9)$$

The slope of the QV-droop characteristic, m_Q, for the inverter-based ESS is the same as that for the inverter-based MS.

C. MATHEMATICAL MODELING OF WOUND-FIELD SYNCHRONOUS GENERATOR-BASED DIESEL GENSET WITH PRIMARY/DROOP CONTROL AND OVERLOAD MITIGATION STRATEGY

The GS comprises an IC engine driven wound-field synchronous generator-based diesel generator. The overload mitigation strategy for GS is exactly the same as that for the inverter-based MS and ESS.

1) PRIMARY/DROOP CONTROL

The primary/droop control and overload mitigation strategy for GS is depicted in Fig. 4. The $P\omega$-droop control for GS can be expressed as follows:

$$\omega = \omega_{base} + \Delta\omega_{adj} + m_P\left(P_{req} - P_{meas}\right) \quad (10)$$

where ω is the frequency of the GS, $\omega_{base} = \omega_0$ is the nominal microgrid frequency, $\Delta\omega_{adj}$ is the frequency adjustment under overload mitigation strategy, m_P is the droop gain (slope of the $P\omega$-droop curve), $P_{req} = P_{set}$ is the GS active power set-point, and P_{meas} is the instantaneous measured active power.

Now, the QV-droop control for GS can be expressed as follows:

$$E_{cmd} = V_{req} - V_{meas} - m_Q Q_{meas} \quad (11)$$

where E_{cmd} is the voltage magnitude command input to the GS exciter controller, $V_{req} = V_{set}$ is the GS line-to-neutral voltage magnitude set-point, V_{meas} is the measured line-to-neutral voltage magnitude, m_Q is the droop gain for GS, and Q_{meas} is the instantaneous measured reactive power. The numerical values of the droop gains, m_P and m_Q, for the GS are exactly the same as those for the inverter-based MS.

There is a voltage control/regulator block adjacent to the QV-droop controller. It receives a voltage error from the QV-droop controller and passes through a PI-controller. The output of the PI-controller is then added up with a feed-forward constant value, V_{base}, which is basically the expected voltage value needed for nominal voltage generation at the terminals. The output of the voltage regulator block, E_{cmd}, is fed into the exciter part of the GS.

The exciter receives inputs from the voltage regulator block and the synchronous generator shaft (i.e., E_{cmd} and ω_r, respectively) and generates DC excitation, V_f, that goes to the synchronous generator field winding.

The other main physical parts of the GS include: governor and IC engine (i.e., prime mover). The governor regulates the mechanical/rotational speed of the synchronous generator primarily by generating a fuel command, F_{cmd}, from the speed error, $(\omega - \omega_r)$, and the measured output power, P_{meas}, where ω is the frequency of the synchronous generator and ω_r is the angular frequency (or rotational speed) of the synchronous generator shaft (or rotor). The speed error is fed into a PI-controller to adjust the torque command, T_{cmd}, as per the load requirement of the synchronous generator. The limiter before the torque command is used to circumvent unrealistic torque commands generation, especially during large load transients. The torque command is then transformed into a fuel command (i.e., $F_{cmd} = K_{tf}T_{cmd}$, where $K_{tf} > 0$ a constant), which is used to decouple the loading of the synchronous generator, and is applied as an input to the IC engine.

The IC engine is the prime mover that mechanically rotates the rotor of the synchronous generator and feeds mechanical energy into it. It generates mechanical power, P_{mech}, from the fuel command. The intermediate steps include the fuel torque, fuel power and friction power losses (i.e., T_F, F_p and P_f, respectively) calculation, as follows:

$$T_F = \eta_{th}K_{fv}K_{ev}F_{cmd} \quad (12)$$
$$F_p = T_F\omega_r \quad (13)$$
$$P_f = K_m\omega_r^2 \quad (14)$$

where η_{th}, K_{fv}, K_{ev} and $K_m > 0$ are constants.

IV. PROPOSED DISTRIBUTED SECONDARY FREQUENCY AND EQUAL POWER SHARING CONTROL STRATEGY

In this section of the article, the proposed consensus-based delay-tolerant distributed finite-time secondary frequency and equal active power sharing control strategy is presented.

Normally, the primary/droop control alone is not sufficient to precisely regulate the frequencies of the DER units back to their nominal values, particularly under load variation. Therefore, an additional secondary control level is needed, besides the primary control, for frequency restoration [11], [12]. In the proposed design, the secondary controller is equipped with a distributed consensus-based controller, which commands each droop-controlled inverter-based DER unit and GS to share equal active power based on the average active load connected, and in turn regulate their frequencies to the nominal value. To fulfill this objective, and inspired by [37], the following distributed nonlinear non-smooth active power consensus algorithm (known as the distributed average

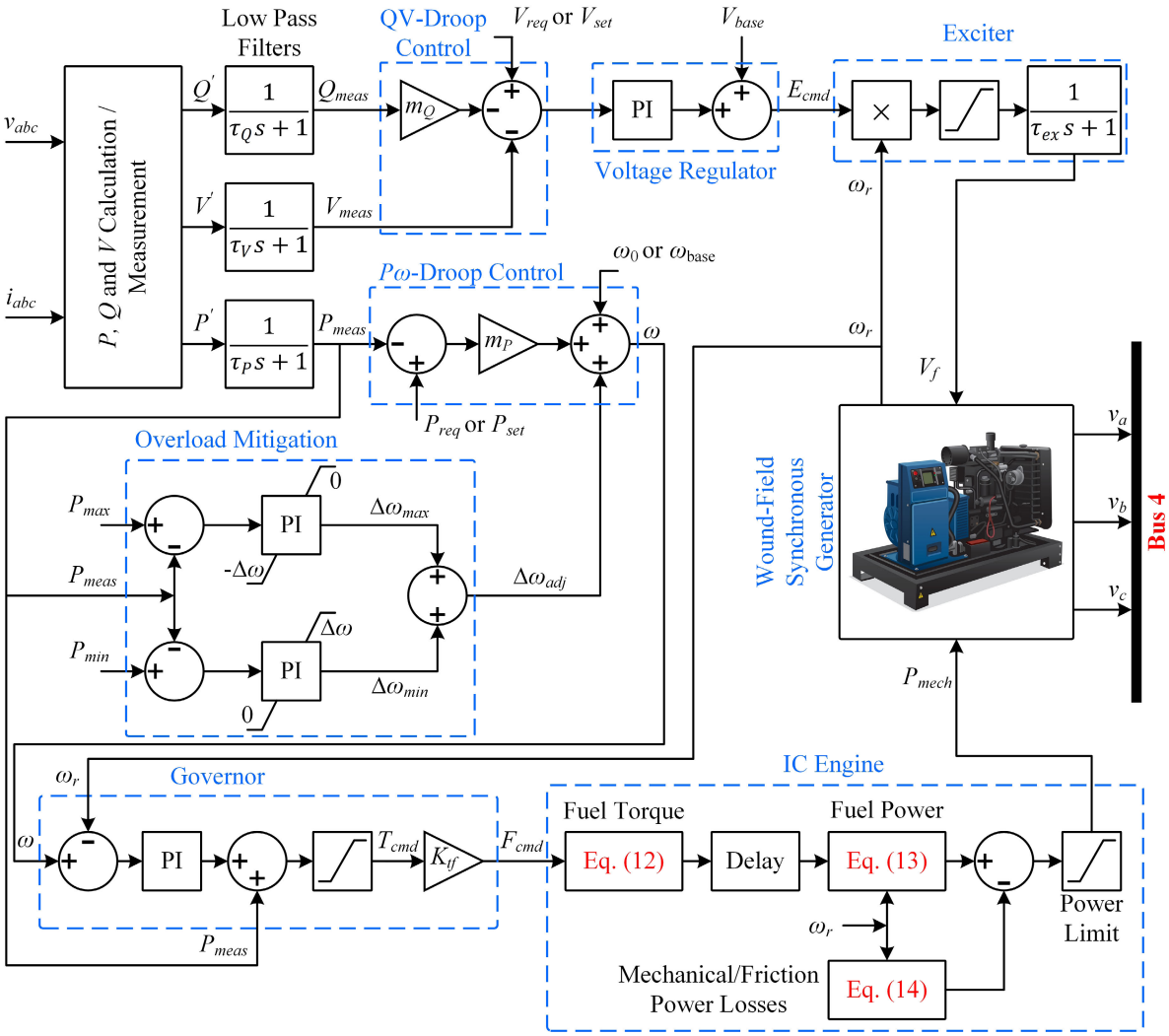

FIGURE 4. Genset with its primary/droop control and overload mitigation strategy.

tracking algorithm) is proposed:

$$\left.\begin{aligned}\dot{v}_i(t) &= -\alpha \sum_{j\in\mathcal{N}_i} \operatorname{sgn}\left[P_{i,meas}(t) - P_{j,meas}(t)\right] \\ P_{i,meas}(t) &= v_i(t) + r_i(t)\end{aligned}\right\} \tag{15}$$

where i is the index set of the DER units, such that $i = \{1, 2, \ldots, N\}$ with $N = 3$, $\alpha > 0$ is a constant, $P_{i,meas}(t) \in \mathbb{R}^N$ is the measured and filtered active power output of the i^{th} DER unit, $v_i(t) \in \mathbb{R}^N$ is an auxiliary (or internal) state variable, $r_i(t)$ is the external reference time-varying signal whose derivative exists and is bounded almost everywhere, and $\operatorname{sgn}(\cdot)$ is the signum function defined component-wise as follows:

$$\operatorname{sgn}(t) = \begin{cases} 1 & \forall \quad t > 0 \\ 0 & \forall \quad t = 0 \\ -1 & \forall \quad t < 0 \end{cases} \tag{16}$$

The external reference signal, $r_i(t)$, is set to the average active load connected, that is, $r_i(t) = P_{Li,avg}(t)$. The objective is to design a distributed algorithm for an agent i, such that all the agents will finally track the average active load, $P_{Li,avg}(t)$, that changes over time. That is, for $i = 1, 2, \ldots, N$,

$$\|P_{i,meas}(t) - P_{Li,avg}(t)\| \to 0, \quad \text{as } t \to \infty$$

The auxiliary state variable, $v_i(t)$ of the i^{th} DER unit, is initialized as follows:

$$v_i(0) = 0 \quad \text{so that} \quad \sum_{i=1}^{N} v_i(0) \quad = 0 \tag{17}$$

From (15) and (17), the following closed-loop system is obtained:

$$\dot{P}_{i,req}(t) = \dot{P}_{i,meas}(t) = \dot{r}_i(t) - \alpha \sum_{j\in\mathcal{N}_i} \operatorname{sgn}\left[P_{i,meas}(t) - P_{j,meas}(t)\right] \tag{18}$$

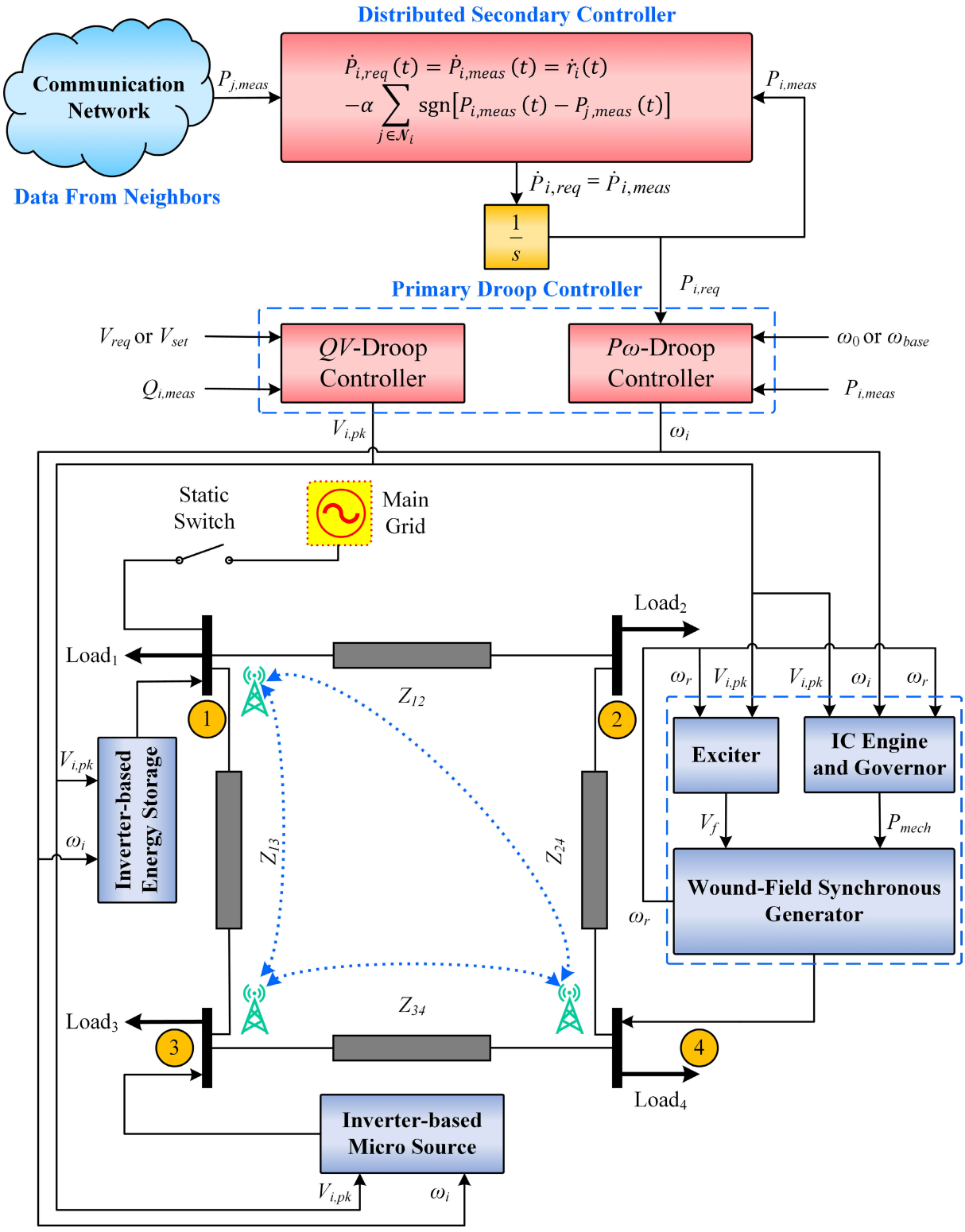

FIGURE 5. Implementation procedure of the proposed secondary control technique.

with the initial conditions $\sum_{i=1}^{N} P_{i,meas}(0) = \sum_{i=1}^{N} r_i(0) = \sum_{i=1}^{N} P_{Li,avg}(0)$.

The implementation procedure of the proposed secondary control technique is illustrated in Fig. 5.

A. CONVERGENCE ANALYSIS

Due to the existence of the discontinuous signum function, the solution of (18) is understood in the Filippov sense [38].

Lemma 1: For system in (18), if the communication graph, $\mathcal{G}$, is connected and $\|P_{i,meas}(t) - P_{j,meas}(t)\| = 0$, for all $i, j = 1, 2, \ldots, N$, then $\|P_{i,meas}(t) - P_{Li,avg}(t)\| = 0$, for all $i = 1, 2, \ldots, N$.

Proof: The main idea behind the algorithm (18) is as follows. First of all, (18) is designed to ensure that $\sum_{i=1}^{N} P_{i,meas}(t) = \sum_{i=1}^{N} P_{Li,avg}(t)$ holds for all time. Note that $\sum_{i=1}^{N} P_{i,meas}(t) = \sum_{i=1}^{N} \nu_i(t) + \sum_{i=1}^{N} P_{Li,avg}(t)$. When the graph, $\mathcal{G}$, is undirected and $\nu_i(0) = 0$,, it implies that $\sum_{i=1}^{N} \nu_i(t) = \sum_{i=1}^{N} \nu_i(0) + \alpha \sum_{i=1}^{N} \sum_{j \in \mathcal{N}_i} \int_0^t \text{sgn}\left[P_{j,meas}(\tau) - P_{i,meas}(\tau)\right] d\tau = 0$. As a result, $\sum_{i=1}^{N} P_{i,meas}(t) = \sum_{i=1}^{N} P_{Li,avg}(t)$ holds for all time. Secondly, when $\mathcal{G}$ is connected, if the algorithm (18) guarantees that all $P_{i,meas}(t)$ approach the same value in finite-time, then it can also be guaranteed that $P_{i,meas}(t)$ also approaches the average active connected load, $r_i(t) = P_{Li,avg}(t)$, in finite-time. □

V. PERFORMANCE VALIDATION THROUGH NUMERICAL SIMULATIONS IN MATLAB/SIMULINK

This section of the article covers the performance validation of the proposed consensus-based distributed secondary frequency and equal power sharing control strategy in Matlab/Simulink through numerical simulations. Five different case studies have been devised to demonstrate the effectiveness and feasibility of the proposed strategy. That is:

Case 1: *Performance evaluation test under the conventional primary/droop control alone*

Case 2: *Performance evaluation test under the proposed secondary control strategy, without plug-and-play and communication time-delay*

Case 3: *Performance evaluation test under the proposed secondary control strategy with plug-and-play event, but without communication time-delay*

Case 4: *Performance evaluation test under the proposed secondary control strategy without plug-and-play event, but with communication time-delay*

Case 5: *Comparison of the proposed secondary control scheme with the existing scheme*

CASE 1: PERFORMANCE EVALUATION TEST UNDER THE CONVENTIONAL PRIMARY/DROOP CONTROL ALONE

To evaluate the performance of the system under primary/droop control alone, the system is simulated with the main grid initially connected and then islanded at $t = 2$ s. The requested voltage levels of all the three DER units are set to 208 V phase-to-phase (i.e., $V_{req_{ESS}} = V_{req_{MS}} = V_{req_{GS}} = 208$ V). The requested active power levels of all the three DER units are set as follows: ESS is set to 1 kW out of 15 kW rating, MS is set to 5 kW out of 15 kW rating, and GS is set to 10 kW out of 12.50 kW rating. The total active load demand till $t = 4$ s is $P_{L,Total} = 28$ kW (with

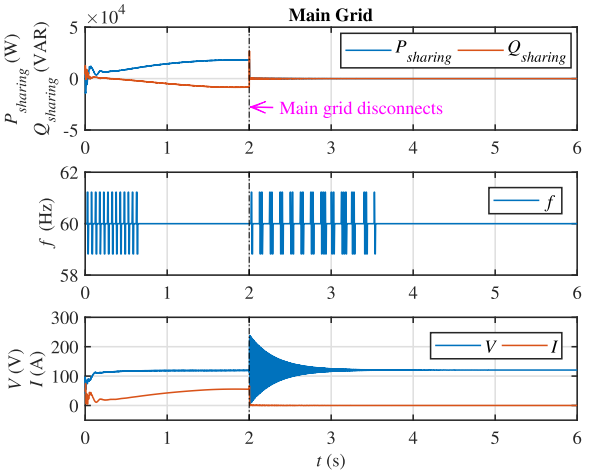

FIGURE 6. Main grid performance before and after disconnection.

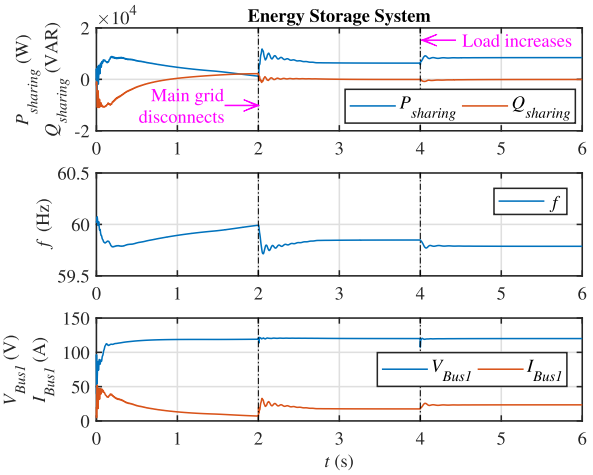

FIGURE 7. ESS performance under droop control alone.

$P_{L,Bus1} = 8$ kW, $P_{L,Bus2} = 4$ kW, $P_{L,Bus3} = 8$ kW, and $P_{L,Bus4} = 8$ kW), which is then increased to 32 kW by a step, by setting $P_{L,Bus2} = 8$ kW, from $t = 4$ s towards the end of simulation.

The behavior of the main grid before and after disconnection is depicted in Fig. 6, while the performance of the ESS, MS and GS, under primary/droop control alone, is illustrated in Figs. 7, 8 and 9, respectively. During transfer to islanding mode, there is a loss of active power from the main grid. The frequency of each DER units is allowed to sag slightly below the nominal frequency ($f_0 = 60$ Hz), adopting the $P\omega$-droop characteristic. Such that, all the DER units immediately ramp up their active powers outputs to compensate for the missing quota of active power from the main grid, without using any explicit communication network between the units. The DER units will continue to ramp up their active power outputs until the present active load demand is fulfilled, at which stage the active power outputs of all the DER units achieve a steady level, as depicted between $t = 2$ s and 4 s. During the load increase event at $t = 4$ s, the two inverter-based DER units (i.e., ESS and MS) further ramp up their active

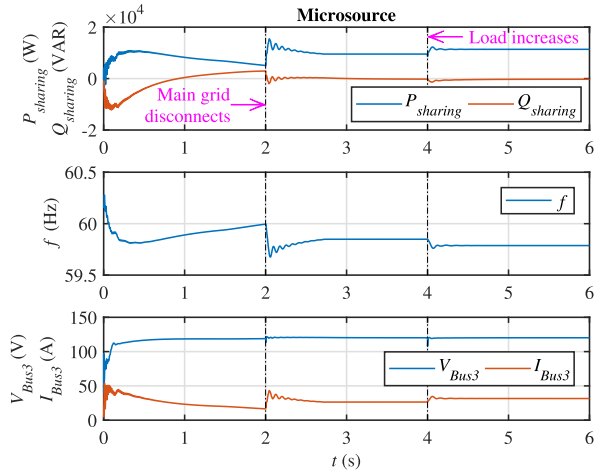

FIGURE 8. MS performance under droop control alone.

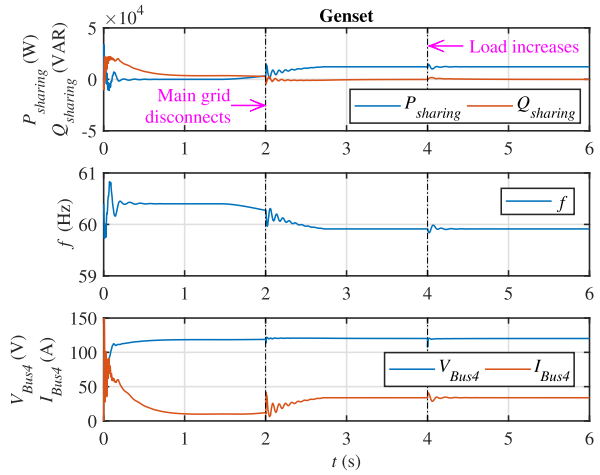

FIGURE 9. GS performance under droop control alone.

power outputs to meet the increased load demand, due to their negligible inertias, by further sagging their frequencies below the nominal frequency. However, due to its high inertia, the GS (rotating synchronous machine-based DER unit) does not pick up load and remains almost at its previous power and frequency level. Note, that the change in frequency of each DER unit is consistent with the specified frequency droop value of 0.5 Hz (i.e., 0.833 %).

In a microgrid with multiple sources, the regulation of the bus voltage levels to a specified constant value results in large circulating VARs between the sources in the system, which decrease the efficiency of the system and increase the components rating. This circulating VARs problem can be minimized by adopting the QV-droop control strategy [39].

Before the main grid disconnection at $t = 2$ s, the circulating VARs are prominent, because the microgrid has to regulate the bus voltage levels to the externally requested voltage levels, V_{req}, (208 V phase-to-phase or 120 V phase-to-neutral). However, after islanding, once the voltage levels are regulated to 120 V, the circulating VARs are decreased to

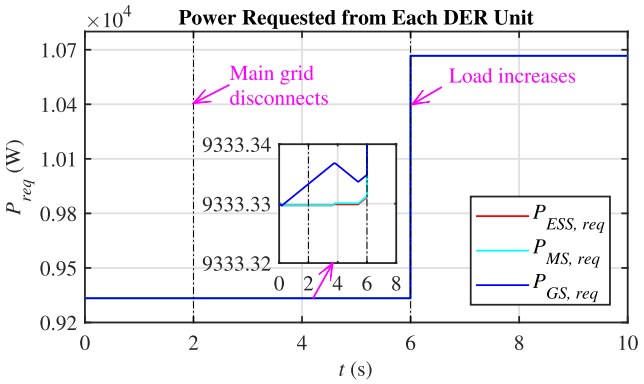

FIGURE 10. Active power requested from each DER unit.

a minimum value. During the load increase event at $t = 4$ s, the voltage levels of the buses also vary slightly, which in turn vary the reactive power sharing output of each DER unit, until the voltages are regulated through the QV-droop controller. Note that the change in voltage level of each bus is consistent with the specified voltage droop value of 5 % (i.e., 6 V for phase-to-neutral voltage).

CASE 2: PERFORMANCE EVALUATION TEST UNDER THE PROPOSED SECONDARY CONTROL STRATEGY, WITHOUT PLUG-AND-PLAY AND COMMUNICATION TIME-DELAY

This case study is constituted to test the performance of the proposed control strategy without giving any consideration to plug-and-play event and communication time-delay.

The total active load demand till $t = 6$ s is $P_{L,Total} = 28$ kW (with $P_{L,Bus1} = 8$ kW, $P_{L,Bus2} = 4$ kW, $P_{L,Bus3} = 8$ kW, and $P_{L,Bus4} = 8$ kW), giving an average load, $P_{Li,avg} = 9333.33$ W, per DER unit. The total load is then increased by a step to, $P_{L,Total} = 32$ kW, by setting $P_{L,Bus2} = 8$ kW from $t = 6$ s towards the end of simulation, giving an average load, $P_{Li,avg} = 10{,}666.67$ W, per DER unit. The constant, α, in (18) is set to 0.001.

As illustrated in Fig. 10, using (18), the requested powers from the DER units are forced to develop average consensus in a finite-time, as depicted in the zoomed-in view. Based on this agreed upon value of the requested powers, all the DER units are forced to dispatch equal active powers before and after the load variation, and track the average active load all the time. Upon the main grid disconnection at $t = 2$ s, the consensus between the power outputs of the DER units is achieved within 2 s. Upon the load increase event at $t = 6$ s, the consensus is achieved at a higher value within 1 s. In both cases, the individual active power output of a DER unit equals the system average load, while the combined active power output of all the three DER units tracks/equals the system total load, as shown in Fig. 11. The overall performance of the ESS, MS and GS is depicted in Figs. 12, 13 and 14, respectively. It is evident, that the frequency is quite accurately regulated to its nominal value (60 Hz), in each case, before and after the load increase event. However, minor transient disturbance can be seen in the frequency upon the

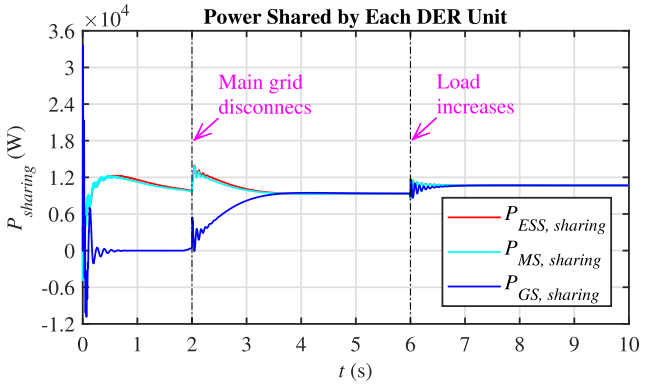

FIGURE 11. Equal active power sharing test for DER units.

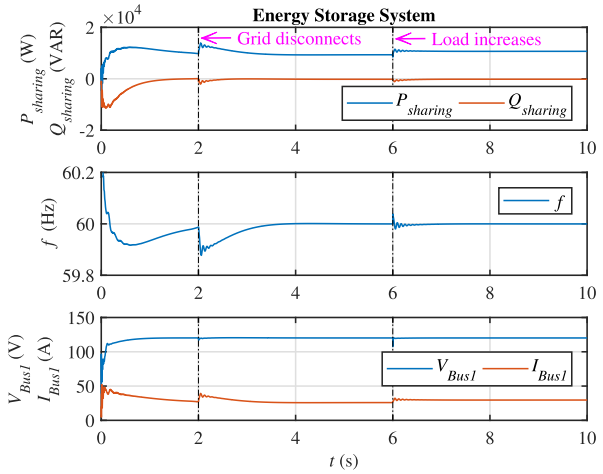

FIGURE 12. Performance of the ESS under the proposed control strategy.

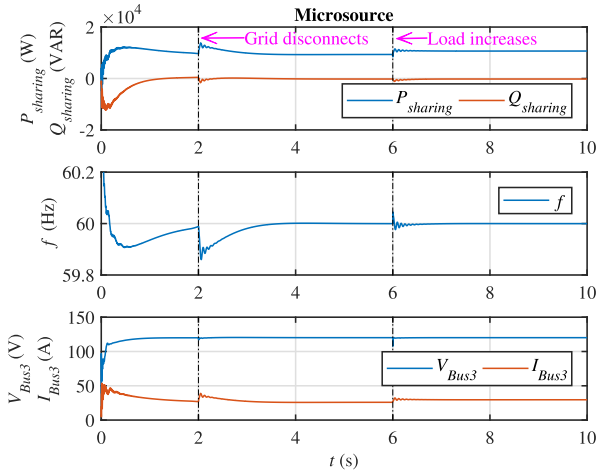

FIGURE 13. Performance of the MS under the proposed control strategy.

load increase event. The reactive power is decreased to a minimum value and the line-to-neutral bus voltage is regulated to its nominal value (120 V). With the increase in load, the bus current as well as the active power dispatch increases.

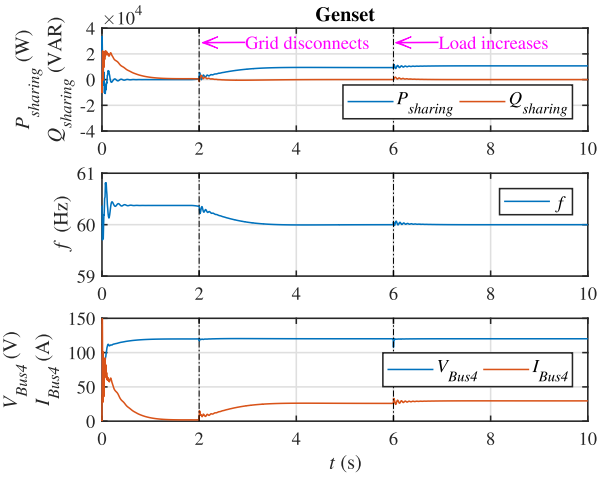

FIGURE 14. Performance of the GS under the proposed control strategy.

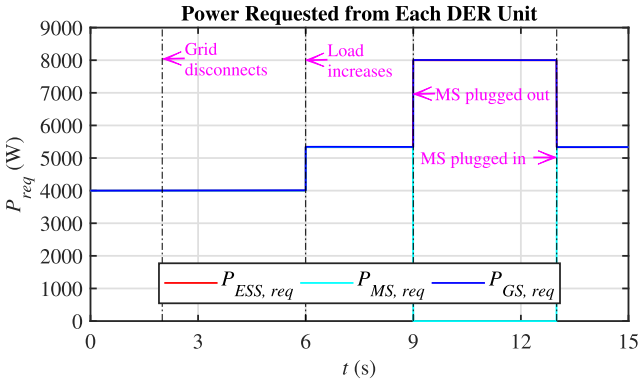

FIGURE 15. Active power requested from each DER unit with plug-and-play event.

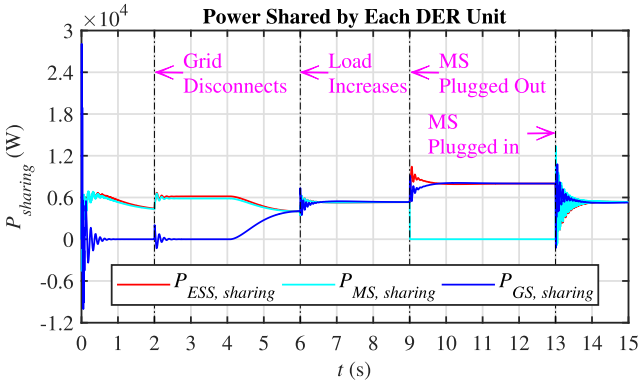

FIGURE 16. Equal active power sharing test for DER units with plug-and-play event.

CASE 3: PERFORMANCE EVALUATION TEST UNDER THE PROPOSED SECONDARY CONTROL STRATEGY WITH PLUG-AND-PLAY EVENT, BUT WITHOUT COMMUNICATION TIME-DELAY

This case study is conducted to analyze the performance of the proposed control strategy under the plug-and-play event, but without giving any consideration to communication time-delay.

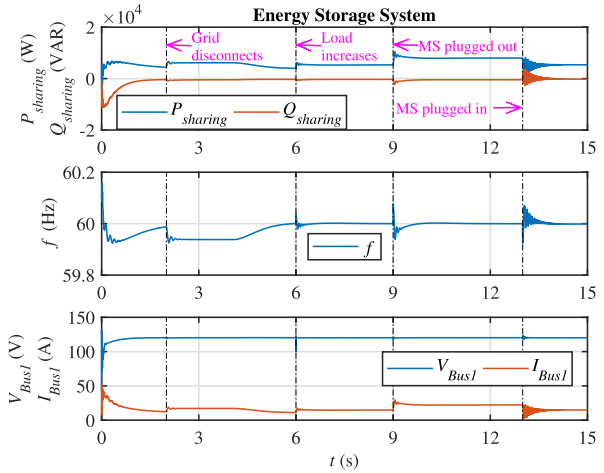

FIGURE 17. Performance of the ESS under the proposed control strategy with plug-and-play event.

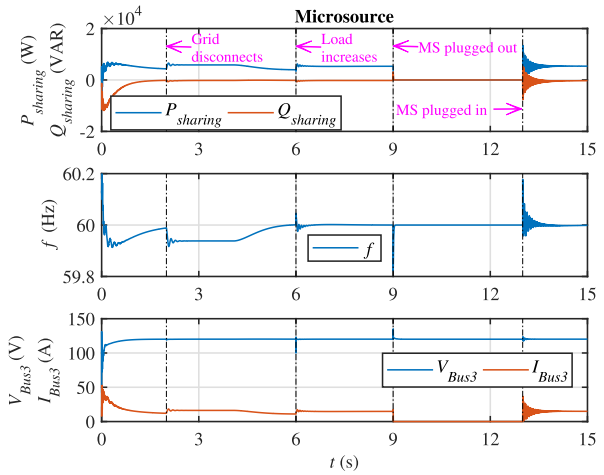

FIGURE 18. Performance of the MS under the proposed control strategy with plug-and-play event.

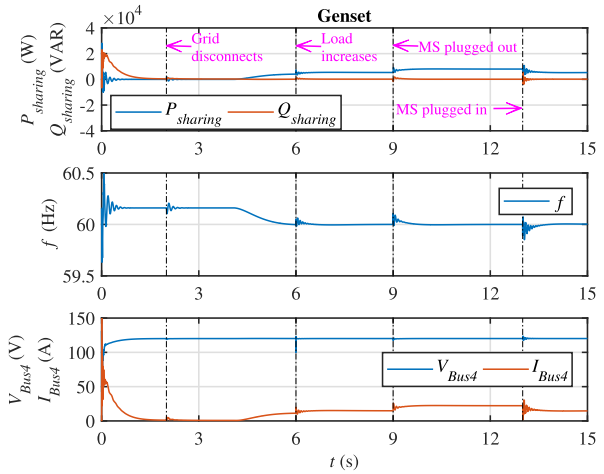

FIGURE 19. Performance of the GS under the proposed control strategy with plug-and-play event.

An important feature of the MAS-based control architecture is to support the plug-and-play feature for the agents. Such that, the system must be capable of

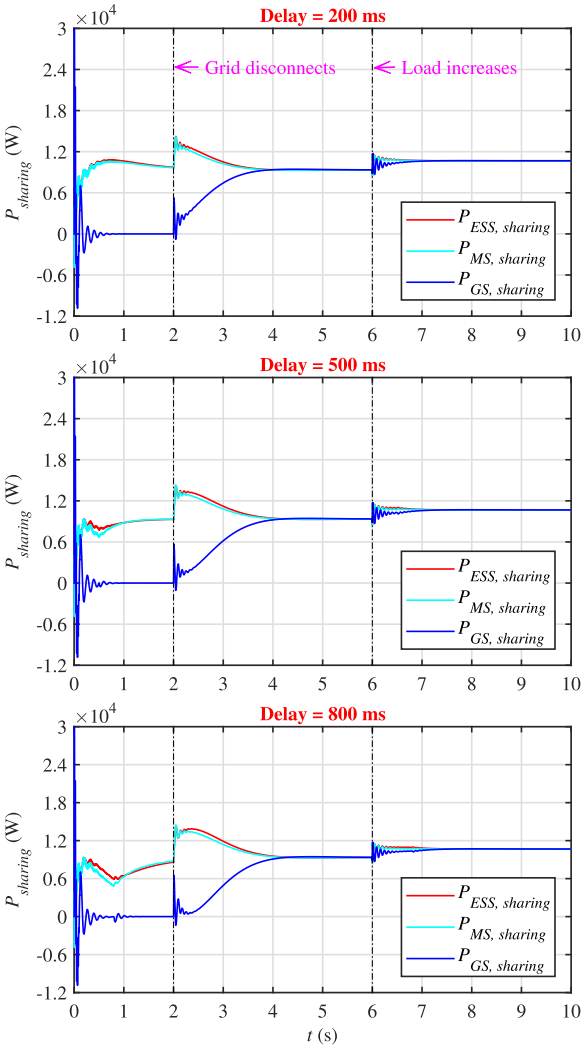

FIGURE 20. Equal active power sharing test for DER units under different communication time-delays.

re-configuring/adapting itself to the change in the communication topology, resulting either from the removal/disconnection of an in-service agent from the system, or then from the addition/integration of an incoming agent to the system [40].

The plug-and-play operation, in this research, is realized by plugging out MS at $t = 9$ s and restoring it at $t = 13$ s. It is worth mentioning, however, that plugging out MS at $t = 9$ s also deactivates the two-way communication links between MS and ESS, and between MS and GS, simultaneously, as shown in Fig. 2.

The total active load demand till $t = 6$ s is $P_{L,Total} = 12$ kW (with $P_{L,Bus1} = 0$ kW, $P_{L,Bus2} = 4$ kW, $P_{L,Bus3} = 4$ kW, and $P_{L,Bus4} = 4$ kW), giving an average load, $P_{Li,avg} = 4$ kW, per DER unit. The total load is then increased by a step to, $P_{L,Total} = 16$ kW, by setting $P_{L,Bus2} = 8$ kW from $t = 6$ s to 9 s, giving an average load, $P_{Li,avg} = 5333.33$ W, per DER unit. At $t = 9$ s, the MS is plugged out, resulting in an average load, $P_{Li,avg} = 8$ kW, per DER unit. At $t = 13$ s, the MS is restored, giving an average load, $P_{Li,avg} = 5333.33$ W,

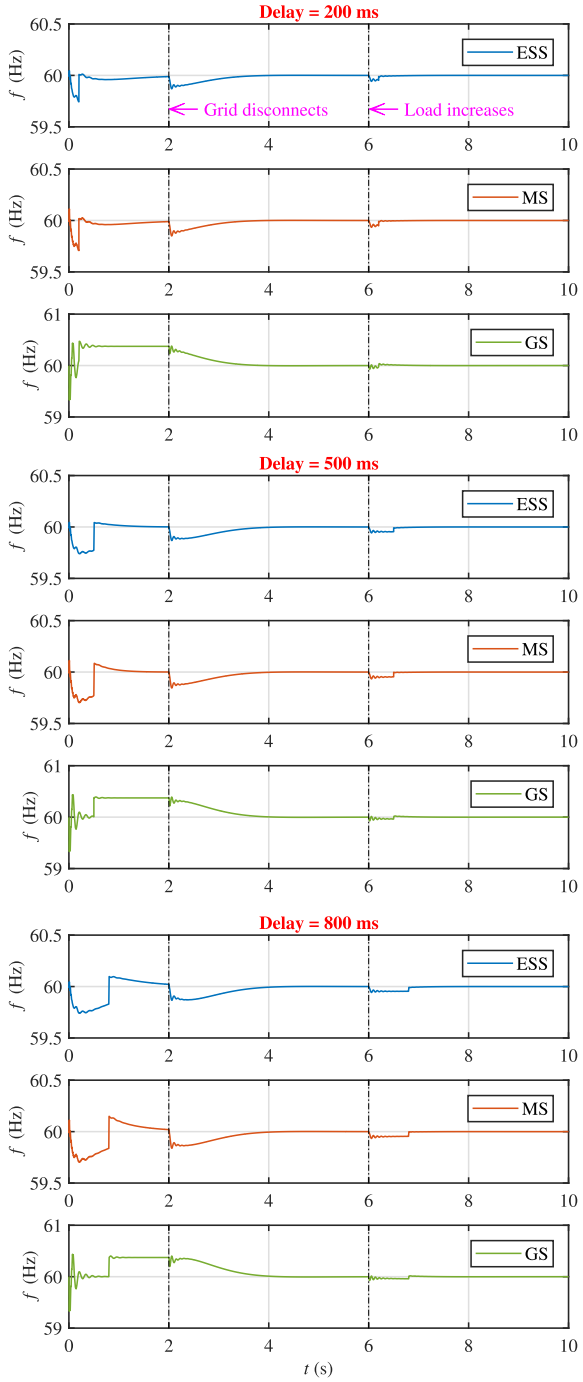

FIGURE 21. Frequency regulation test for DER units under different communication time-delays.

per DER unit, and is kept delivering power till the end of simulation.

As shown in Fig. 15, using (18), the requested powers from the DER units are again forced to develop average consensus in a finite-time. Upon the main grid disconnection at $t = 2$ s, the consensus between the power outputs of the DER units is developed at 4 kW. Upon the load increase event, the consensus is developed at an increased value of 5333 W. Upon taking MS out-of-service, the remaining DER units

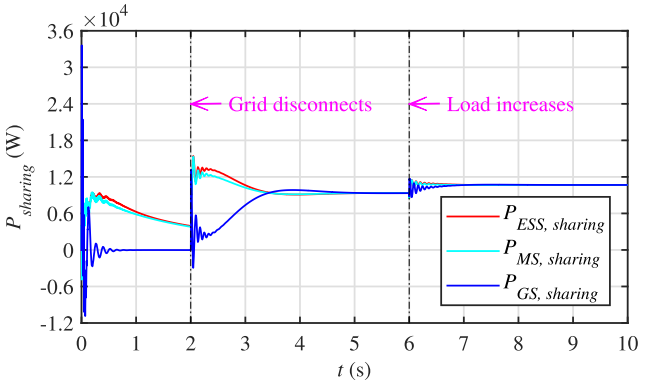

FIGURE 22. Equal active power sharing test for DER units using [30]–[32].

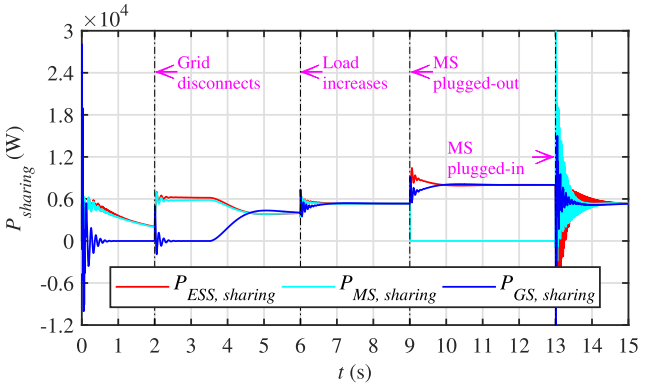

FIGURE 23. Equal active power sharing test for DER units under plug-and-play event using [30]–[32].

(i.e., ESS and GS) have to ramp up their active power outputs to compensate for the power previously delivered by all the three DER units collectively. Hence, consensus is achieved at a further increased value of 8 kW. While upon restoring MS, consensus is developed back at a lower value of 5333 W. In each case, the individual active power output of a DER unit equals the system average load, while the combined active power output of all the three DER units tracks/equals the system total load, as illustrated in Fig. 16.

Figures 17, 18 and 19, respectively, depict the overall performance of the ESS, MS and GS. It can be seen that the frequency is quite accurately regulated to its nominal value (60 Hz), in each case. Both the load increase and plug-and-play events render minor transient disturbances in the frequency. The reactive power is decreased to a minimum value, and the line-to-neutral bus voltage is regulated to its nominal value (120 V).

CASE 4: PERFORMANCE EVALUATION TEST UNDER THE PROPOSED SECONDARY CONTROL STRATEGY WITHOUT PLUG-AND-PLAY EVENT, BUT WITH COMMUNICATION TIME-DELAY

The robustness of the proposed control strategy to communication time-delays is tested under different time-delays (i.e., 200 ms, 500 ms and 800 ms), in this section. It can be seen in Figs. 20 and 21 that the closed-loop system response

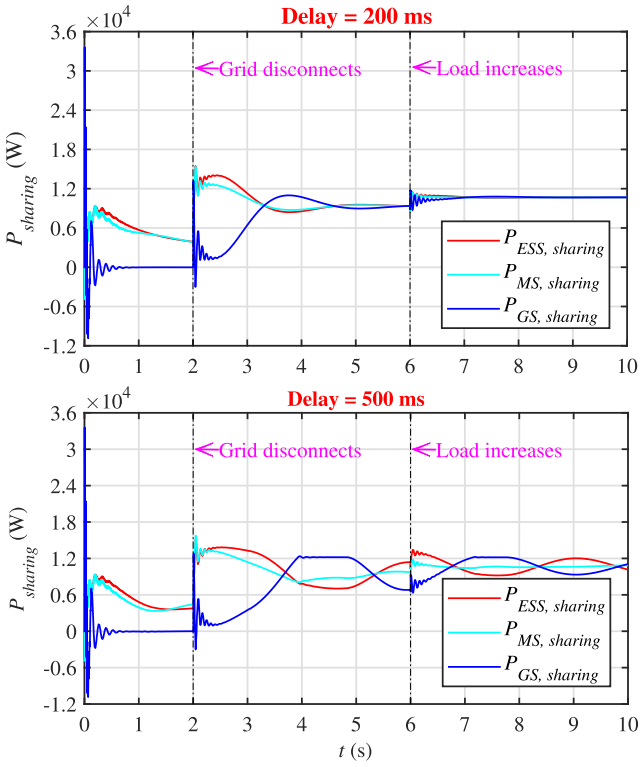

FIGURE 24. Equal active power sharing test for DER units under different communication time-delays using [30]–[32].

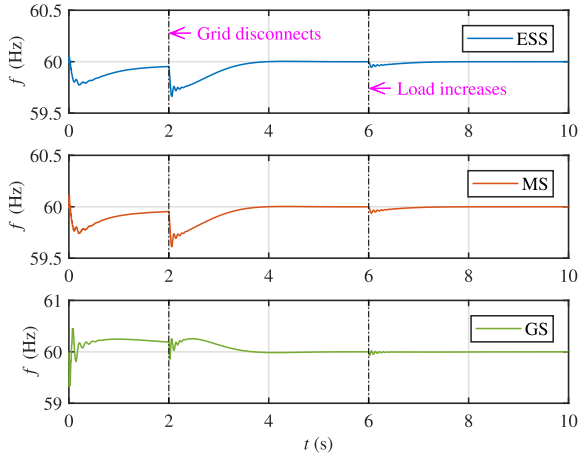

FIGURE 25. Frequency regulation test for DER units using [30]–[32].

(i.e., $P_{sharing}$ and f of DER units) becomes oscillatory and the convergence becomes slow under communication time-delays. Such that, greater the time-delay, greater will be the oscillation and slower will be convergence, and vice versa. However, the proposed strategy is still capable of fulfilling its objectives by successfully tolerating both small and large communication time-delays.

CASE 5: COMPARISON OF THE PROPOSED SECONDARY CONTROL SCHEME WITH THE EXISTING SCHEME

The proposed control scheme is further tested against the existing distributed equal active power sharing scheme, found

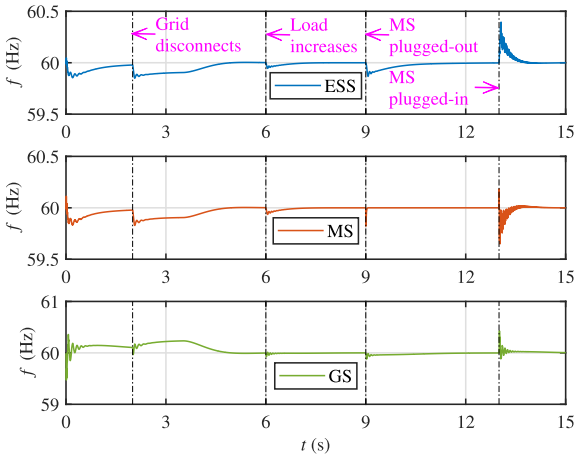

FIGURE 26. Frequency regulation test for DER units under plug-and-play event using [30]–[32].

TABLE 1. Line impedances, coupling inductances and coupling capacitor of the test microgrid.

Line Impedance	$R\ (\Omega)$	$X_L\ (\Omega)$	$X_C\ (\Omega)$
Z_1	0.0934	0.0255	2894.30
Z_2	0.00281	0.000679	2894.30
Z_3	0	3.77	0
Z_4	0	3.77	0
Z_g	0	0	26.53
Z_{12}	0.027352	0.0066	288.60
Z_{13}	0.0137	0.0033	577.20
Z_{24}	0.01688	0.00407	336.70
Z_{34}	0.0026	0.00064	2020.10

in [30]–[32], and expressed as follows.

$$\dot{P}_{i,req}\,(t) = \dot{P}_{i,meas}\,(t) = -\alpha \sum_{j\in\mathcal{N}_i}\Big[P_{i,meas}\,(t) - P_{j,meas}\,(t)\Big] \quad (19)$$

As depicted in Figs. 22-24, the control scheme presented in [30]–[32] exhibits a slower convergence and larger deviations in case of equal active power sharing, than the proposed control scheme depicted in Figs. 11, 16, and 20 under the same conditions. These deviations in power sharing are quite prominent in case of plug-and-play operation, as shown in Fig. 23. Similarly, in case of communication time-delays, shown in Fig. 24, the scheme presented in [30]–[32], exhibits larger oscillations in power sharing under large time-delays (i.e., 500 ms), than the proposed control scheme depicted in Fig. 20, and the consensus/convergence is not achieved even after $t = 10$ s.

Similarly, in case of frequency regulation, the scheme presented in [30]–[32], exhibits much larger deviations, as depicted in Figs. 25-27 than the proposed scheme depicted in Figs. 12-14, 17-19, and 21 under the same conditions. Again, these deviations are easily noticeable under plug-and-play operation, as illustrated in Fig. 26. While in

TABLE 2. Transformer specifications of the test microgrid.

TAG	Rating (kVA)	Frequency (Hz)	Primary Side			Secondary Side		
			V_{ph-ph} (V)	R (Ω)	X_L (Ω)	V_{ph-ph} (V)	R (Ω)	X_L (Ω)
TF_1	2500	60	4160	0.04706	0.1882	480	0.000627	0.0025068
TF_2	75	60	480	0.0169	0.0676	208	0.0003	0.0127
TF_3	45	60	208	0.02688	0.1075	208	0.005047	0.0201
TF_4	45	60	208	0.02688	0.1075	208	0.005047	0.0201
TF_5	45	60	208	0.02688	0.1075	208	0.005047	0.0201

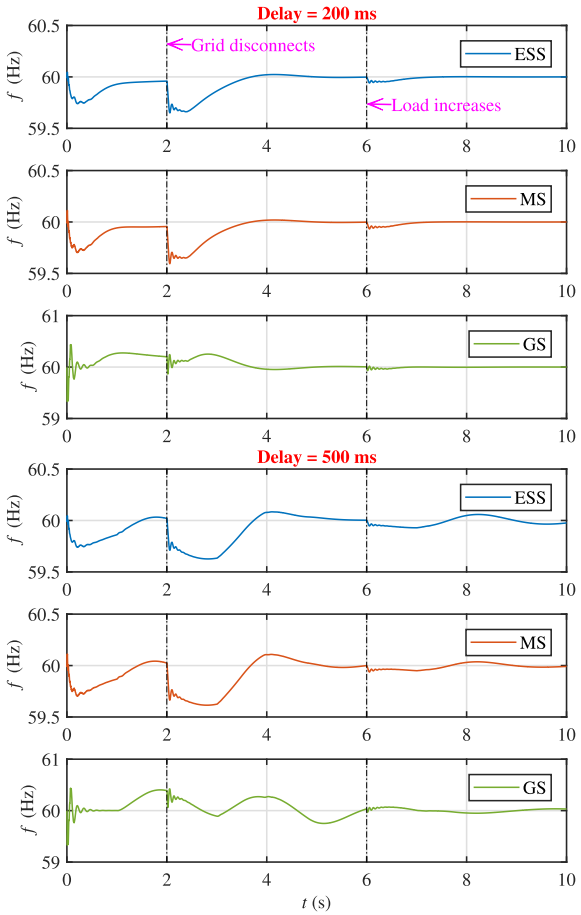

FIGURE 27. Frequency regulation test for DER units under different communication time-delays using [30]–[32].

TABLE 3. Specifications of the inverter-interfaced energy storage system and microsource of the test microgrid.

Microsource		Energy Storage System	
Quantity	Value	Quantity	Value
S_{base}	15 kVA	S_{base}	15 kVA
V_{base}	208 V	V_{base}	208 V
V_{DC}	750 V	V_{DC}	750 V
$f_{base} = f_0$	60 Hz	$f_{base} = f_0$	60 Hz
Δf	0.50 Hz	Δf	0.50 Hz
$\omega_{base} = \omega_0$	$\begin{cases} 2\pi f_{base} \\ 377\ \text{rad/s} \end{cases}$	$\omega_{base} = \omega_0$	377 rad/s
$\Delta\omega$	$\begin{cases} 2\pi\Delta f \\ \pi\ \text{rad/s} \end{cases}$	$\Delta\omega$	π rad/s
P_{max}	$\begin{cases} 15\ \text{kW} \\ 1\ \text{pu} \end{cases}$	P_{max}	$\begin{cases} 15\ \text{kW} \\ 1\ \text{pu} \end{cases}$
P_{min}	0 kW	P_{min}	$\begin{cases} -2.50\ \text{kW} \\ -0.1667\ \text{pu} \end{cases}$
V_{req}	$\begin{cases} 208\ \text{V} \\ 1\ \text{pu} \end{cases}$	V_{req}	$\begin{cases} 208\ \text{V} \\ 1\ \text{pu} \end{cases}$
$K_{P_{pro}}$	3	$K_{P_{pro}}$	3
$K_{P_{int}}$	30	$K_{P_{int}}$	30
$K_{V_{pro}}$	0.01	$K_{V_{pro}}$	0.01
$K_{V_{int}}$	5	$K_{V_{int}}$	5
m_P	π	m_P	2.6928
m_Q	0.05	m_Q	0.05
τ_V, τ_P, τ_Q	0.01	τ_V, τ_P, τ_Q	0.01

case of communication time-delays, the scheme presented in [30]–[32], as shown in Fig. 27, finds it difficult to converge the frequencies to their nominal values under large time-delays (i.e., 500 ms), than the proposed control scheme depicted in Fig. 21, still precisely regulating the frequencies.

VI. CONCLUSION

In this article, a fully-distributed and delay-tolerant robust secondary control scheme is proposed for droop-controlled AC microgrids. The stated strategy is inspired by the cooperative control concept of multi-agent systems. It considers the hierarchical control structure of the DER units. Owing to the fully-distributed configuration of the proposed control strategy, each DER unit in the test microgrid requires only its own information and information of its neighbors. This not only minimizes the overall bandwidth requirement and cost of the underlying communication network, but also increases the reliability of the microgrid operation. The proposed technique ensures equal active power sharing between three DER units by tracking the time-varying average load, with a finite-time convergence. Consequently, the frequencies of the DER units are regulated to their nominal values. Additionally, the proposed strategy renders the plug-and-play capability for DER units, and demonstrates significant robustness against load disturbances and, both small and large, communication time-delays. A notable feature of the proposed control scheme is that it ensures equal active power sharing and frequency regulation using a single control protocol for each DER unit as compared to the concepts reported in [30]–[32], where a separate control methodology has been used for both

TABLE 4. Specifications of the genset of the test microgrid.

Genset (Synchronous Generator, Governor, IC Engine and Exciter)			
Quantity	Value	Quantity	Value
S_{base}	12.50 kVA	X_q	0.533
V_{base}	208 V	X''_q	0.051
$f_{base} = f_0$	60 Hz	X_l	0.037
Δf	0.50 Hz	T'_d	0.35523
$\omega_{base} = \omega_0$	$2\pi f_{base}$ / 377 rad/s	T''_d	0.00015
$\Delta\omega$	$2\pi\Delta f$ / π rad/s	T''_q	0.0067
P_{max}	12.50 kW / 1 pu	R_s	0.0217 pu
P_{min}	0 kW	$H(s)$	0.19
V_{req}	208 V / 1 pu	p	2
$K_{P_{pro}}$	3	K_{G_p}	10
$K_{P_{int}}$	30	K_{G_i}	20
$K_{V_{pro}}$	1000	K_{tf}	0.625
$K_{V_{int}}$	10	K_{ev}	11.8238
m_P	π	K_{fv}	3600
m_Q	0.05	η_{thr}	0.47
$\tau_V,\ \tau_P,\ \tau_Q$	0.01	τ_d	0.022 s
X_d	1.204	K_m	0.36
X'_d	0.125	τ_{ex}	0.001 s
X''_d	0.056	...	...

purposes. The performance and efficacy of the proposed strategy is validated through exhaustive numerical simulations performed in Matlab/Simulink on an AC microgrid testbench comprising three DER units. The proposed strategy exhibits a superior performance as compared to the existing control strategy in this area.

APPENDIX
PARAMETERS OF THE WHOLE SYSTEM

See Tables 1–4.

REFERENCES

[1] A. Afshari, M. Karrari, H. R. Baghaee, and G. B. Gharehpetian, "Resilient cooperative control of AC microgrids considering relative state-dependent noises and communication time-delays," *IET Renew. Power Gener.*, vol. 14, no. 8, pp. 1321–1331, Jun. 2020.

[2] A. Afshari, M. Karrari, H. R. Baghaee, G. B. Gharehpetian, and S. Karrari, "Cooperative fault-tolerant control of microgrids under switching communication topology," *IEEE Trans. Smart Grid*, vol. 11, no. 3, pp. 1866–1879, May 2020.

[3] F. Katiraei, M. R. Iravani, and P. W. Lehn, "Micro-grid autonomous operation during and subsequent to islanding process," *IEEE Trans. Power Del.*, vol. 20, no. 1, pp. 248–257, Jan. 2005.

[4] M. Cucuzzella, S. Trip, C. De Persis, X. Cheng, A. Ferrara, and A. van der Schaft, "A robust consensus algorithm for current sharing and voltage regulation in DC microgrids," *IEEE Trans. Control Syst. Technol.*, vol. 27, no. 4, pp. 1583–1595, Jul. 2019.

[5] N. M. Dehkordi, H. R. Baghaee, N. Sadati, and J. M. Guerrero, "Distributed noise-resilient secondary voltage and frequency control for islanded microgrids," *IEEE Trans. Smart Grid*, vol. 10, no. 4, pp. 3780–3790, Jul. 2019.

[6] R. Perez-Ibacache, C. A. Silva, and A. Yazdani, "Linear state-feedback primary control for enhanced dynamic response of AC microgrids," *IEEE Trans. Smart Grid*, vol. 10, no. 3, pp. 3149–3161, May 2019.

[7] H. R. Baghaee, M. Mirsalim, G. B. Gharehpetian, and H. A. Talebi, "Unbalanced harmonic power sharing and voltage compensation of microgrids using radial basis function neural network-based harmonic power-flow calculations for distributed and decentralised control structures," *IET Gener., Transmiss. Distrib.*, vol. 12, no. 8, pp. 1518–1530, Nov. 2017.

[8] J. A. P. Lopes, C. L. Moreira, and A. G. Madureira, "Defining control strategies for MicroGrids islanded operation," *IEEE Trans. Power Syst.*, vol. 21, no. 2, pp. 916–924, May 2006.

[9] M. Cucuzzella, G. P. Incremona, and A. Ferrara, "Decentralized sliding mode control of islanded AC microgrids with arbitrary topology," *IEEE Trans. Ind. Electron.*, vol. 64, no. 8, pp. 6706–6713, Aug. 2017.

[10] M. Savaghebi, A. Jalilian, J. C. Vasquez, and J. M. Guerrero, "Secondary control scheme for voltage unbalance compensation in an islanded droop-controlled microgrid," *IEEE Trans. Smart Grid*, vol. 3, no. 2, pp. 797–807, Jun. 2012.

[11] H. R. Baghaee, G. B. Gharehpetian, and M. Mirsalim, "Real-time verification of new controller to improve small/large-signal stability and fault ride-through capability of multi-DER microgrids," *IET Gener., Transmiss. Distrib.*, vol. 10, no. 12, pp. 3068–3084, Sep. 2016.

[12] J. M. Guerrero, M. Chandorkar, T.-L. Lee, and P. C. Loh, "Advanced control architectures for intelligent microgrids—Part I: Decentralized and hierarchical control," *IEEE Trans. Ind. Electron.*, vol. 60, no. 4, pp. 1254–1262, Apr. 2013.

[13] J. Hu and P. Bhowmick, "A consensus-based robust secondary voltage and frequency control scheme for islanded microgrids," *Int. J. Electr. Power Energy Syst.*, vol. 116, Mar. 2020, Art. no. 105575.

[14] Y. Seyedi, H. Karimi, and J. M. Guerrero, "Centralized disturbance detection in smart microgrids with noisy and intermittent synchrophasor data," *IEEE Trans. Smart Grid*, vol. 8, no. 6, pp. 2775–2783, Nov. 2017.

[15] J. Lai, H. Zhou, X. Lu, X. Yu, and W. Hu, "Droop-based distributed cooperative control for microgrids with time-varying delays," *IEEE Trans. Smart Grid*, vol. 7, no. 4, pp. 1775–1789, Jul. 2016.

[16] G. A. Pagani and M. Aiello, "Towards decentralization: A topological investigation of the medium and low voltage grids," *IEEE Trans. Smart Grid*, vol. 2, no. 3, pp. 538–547, Sep. 2011.

[17] P. Garcia-Trivino, J. P. Torreglosa, L. M. Fernandez-Ramirez, and F. Jurado, "Decentralized fuzzy logic control of microgrid for electric vehicle charging station," *IEEE J. Emerg. Sel. Topics Power Electron.*, vol. 6, no. 2, pp. 726–737, Jun. 2018.

[18] Q. Li, C. Peng, M. Wang, M. Chen, J. M. Guerrero, and D. Abbott, "Distributed secondary control and management of islanded microgrids via dynamic weights," *IEEE Trans. Smart Grid*, vol. 10, no. 2, pp. 2196–2207, Mar. 2019.

[19] N. L. Diaz, J. C. Vasquez, and J. M. Guerrero, "A communication-less distributed control architecture for islanded microgrids with renewable generation and storage," *IEEE Trans. Power Electron.*, vol. 33, no. 3, pp. 1922–1939, Mar. 2018.

[20] X. Lu, R. Lu, S. Chen, and J. Lu, "Finite-time distributed tracking control for multi-agent systems with a virtual leader," *IEEE Trans. Circuits Syst. I, Reg. Papers*, vol. 60, no. 2, pp. 352–362, Feb. 2013.

[21] X. Lu, S. Chen, and J. Lü, "Finite-time tracking for double integrator multi-agent systems with bounded control input," *IET Control Theory Appl.*, vol. 7, no. 11, pp. 1562–1573, Jul. 2013.

[22] A. Bidram, A. Davoudi, and F. L. Lewis, "A multiobjective distributed control framework for islanded AC microgrids," *IEEE Trans. Ind. Informat.*, vol. 10, no. 3, pp. 1785–1798, Aug. 2014.

[23] A. Bidram, F. L. Lewis, and A. Davoudi, "Distributed control systems for small-scale power networks: Using multiagent cooperative control theory," *IEEE Control Syst. Mag.*, vol. 34, no. 6, pp. 56–77, Dec. 2014.

[24] N. M. Dehkordi, N. Sadati, and M. Hamzeh, "Distributed robust finite-time secondary voltage and frequency control of islanded microgrids," *IEEE Trans. Power Syst.*, vol. 32, no. 5, pp. 3648–3659, Sep. 2017.

[25] A. Bidram, A. Davoudi, F. L. Lewis, and J. M. Guerrero, "Distributed cooperative secondary control of microgrids using feedback linearization," *IEEE Trans. Power Syst.*, vol. 28, no. 3, pp. 3462–3470, Aug. 2013.

[26] A. Bidram, F. L. Lewis, Z. Qu, and A. Davoudi, "Secondary control of microgrids based on distributed cooperative control of multi-agent systems," *IET Gener., Transmiss. Distrib.*, vol. 7, no. 8, pp. 822–831, Aug. 2013.

[27] N. M. Dehkordi, N. Sadati, and M. Hamzeh, "Fully distributed cooperative secondary frequency and voltage control of islanded microgrids," *IEEE Trans. Energy Convers.*, vol. 32, no. 2, pp. 675–685, Jun. 2017.
[28] S. Liu, X. Wang, and P. X. Liu, "Impact of communication delays on secondary frequency control in an islanded microgrid," *IEEE Trans. Ind. Electron.*, vol. 62, no. 4, pp. 2021–2031, Apr. 2015.
[29] J. W. Simpson-Porco, Q. Shafiee, F. Dorfler, J. C. Vasquez, J. M. Guerrero, and F. Bullo, "Secondary frequency and voltage control of islanded microgrids via distributed averaging," *IEEE Trans. Ind. Electron.*, vol. 62, no. 11, pp. 7025–7038, Nov. 2015.
[30] S. Ullah, L. Khan, R. Badar, A. Ullah, F. W. Karam, Z. A. Khan, and A. U. Rehman, "Consensus based SoC trajectory tracking control design for economic-dispatched distributed battery energy storage system," *PLoS ONE*, vol. 15, no. 5, May 2020, Art. no. e0232638.
[31] D. H. Nguyen and J. Khazaei, "Multiagent time-delayed fast consensus design for distributed battery energy storage systems," *IEEE Trans. Sustain. Energy*, vol. 9, no. 3, pp. 1397–1406, Jul. 2018.
[32] J. Khazaei and D. H. Nguyen, "Multi-agent consensus design for heterogeneous energy storage devices with droop control in smart grids," *IEEE Trans. Smart Grid*, vol. 10, no. 2, pp. 1395–1404, Mar. 2019.
[33] T. K. Roy, M. A. Mahmud, A. M. T. Oo, R. Bansal, and M. E. Haque, "Nonlinear adaptive backstepping controller design for three-phase grid-connected solar photovoltaic systems," *Electr. Power Compon. Syst.*, vol. 45, no. 20, pp. 2275–2292, Dec. 2017.
[34] M. J. Erickson and R. H. Lasseter, "Integration of battery energy storage element in a CERTS microgrid," in *Proc. IEEE Energy Convers. Congr. Expo.*, Atlanta, GA, USA, Sep. 2010, pp. 2570–2577.
[35] R. H. Lasseter and P. Piagi, "Control and design of microgrid components," Power Syst. Eng. Res. Center (PSERC), Univ. Wisconsin-Madison, Madison, WI, USA, Tech. Rep., Jan. 2006. Accessed: Oct. 20, 2020. [Online]. Available: https://certs.lbl.gov/sites/all/files/ctrl-design-microgrid-components.pdf
[36] W. Du and R. H. Lasseter, "Overload mitigation control of droop-controlled grid-forming sources in a microgrid," in *Proc. IEEE Power Energy Soc. Gen. Meeting*, Chicago, IL, USA, Jul. 2017, pp. 1–5.
[37] F. Chen, Y. Cao, and W. Ren, "Distributed average tracking of multiple time-varying reference signals with bounded derivatives," *IEEE Trans. Autom. Control*, vol. 57, no. 12, pp. 3169–3174, Dec. 2012.
[38] J. Cortes, "Discontinuous dynamical systems," *IEEE Control Syst. Mag.*, vol. 28, no. 3, pp. 36–73, Jun. 2008.
[39] S. Krishnamurthy, T. M. Jahns, and R. H. Lasseter, "The operation of diesel gensets in a CERTS microgrid," in *Proc. IEEE Power Energy Soc. Gen. Meeting Convers. Del. Electr. Energy 21st Century*, Pittsburgh, PA, USA, Jul. 2008, pp. 1–8.
[40] T.-L. Nguyen, E. Guillo-Sansano, M. Syed, V.-H. Nguyen, S. Blair, L. Reguera, Q.-T. Tran, R. Caire, G. Burt, C. Gavriluta, and N.-A. Luu, "Multi-agent system with plug and play feature for distributed secondary control in microgrid–controller and power hardware-in-the-loop implementation," *Energies*, vol. 11, no. 12, p. 3253, Nov. 2018.

SHAFAAT ULLAH was born in Lakki Marwat, Pakistan. He received the B.Sc. and M.Sc. degree in electrical engineering from the University of Engineering and Technology Peshawar, Bannu Campus, Bannu, Pakistan, in 2007 and 2013, respectively. He is currently pursuing the Ph.D. degree in electrical engineering with COMSATS University Islamabad, Abbottabad Campus, Abbottabad, Pakistan.

He has served as an Assistant Director for the Pakistan Council of Renewable Energy Technologies (PCRET), and as an Assistant Manager (Operation)/Junior Engineer (Electrical) for Lahore Electric Supply Company (LESCO), Pakistan. He is also serving as an Assistant Professor (on Ph.D. Study Leave) with the Department of Electrical Engineering, University of Engineering and Technology Peshawar. His research interests include photovoltaics, wind energy conversion systems, and distributed control of multi-agent systems-based smart grids.

LAIQ KHAN received the B.Sc. degree (Hons.) in electrical engineering from the University of Engineering and Technology Peshawar, Peshawar, Pakistan, in 1996, and the M.S.-leading-to-Ph.D. degree in power system dynamics and control from the University of Strathclyde, Glasgow, U.K., in 2003.

Before Ph.D. degree, he served for Siemens Pakistan as a Field Engineer, for two years. He served as an Assistant Professor for the Faculty of Electronic Engineering, Ghulam Ishaq Khan Institute of Engineering Sciences and Technology, Swabi, Pakistan, till 2008. Then, he joined the Faculty of Electrical Engineering, COMSATS University Islamabad, Abbottabad Campus, Pakistan, and served as an Associate Professor. He also served as a Professor for Islamic University Madinah, Saudi Arabia, for three years. He is currently a Professor of power system dynamics and control with COMSATS University Islamabad, Abbottabad Campus. He has published more than hundred articles in highly reputable international conferences and peer-reviewed impact factor journals. His research interests include power system stability and control using PSSs, FACTS controllers and HVDC, robust control theory, intelligent control systems, nonlinear adaptive intelligent control and adaptive predictive intelligent control, fault tolerant control, power system planning and advanced optimization techniques, nonlinear control of wecs, photovoltaic systems, micro-grids, and smart-grids.

IRFAN SAMI received the B.Sc. degree in electrical engineering from the University of Engineering and Technology Peshawar, Bannu Campus, Pakistan, in 2016, and the M.Sc. degree in electrical engineering from COMSATS University Islamabad, Abbottabad Campus, Abbottabad, Pakistan, in 2019. He is currently pursuing the Ph.D. degree in electrical engineering with Chung-Ang University, Seoul, South Korea. His research interests include electric drives, renewable energies, and electrical machines design.

NASIM ULLAH received the Ph.D. degree in mechatronic engineering from Beihang University, Beijing, China, in 2013. From September 2006 to 2010, he was a Senior Design Engineer with IICS, Pakistan. He is currently working as an Associate Professor of Electrical Engineering with TAIF University KSA. His research interests include renewable energy, flight control systems, integer and fractional order modeling of dynamic systems, integer/fractional order adaptive robust control methods, Fuzzy/NN, hydraulic and electrical servos, epidemic, and vaccination control strategies.